



**Effect of individual differences on the jamming transition in traffic flow**Yi-Chieh Lai  and Kuo-An Wu <sup>\*</sup>*Department of Physics, National Tsing Hua University, 30013 Hsinchu, Taiwan*

(Received 8 February 2021; revised 17 June 2021; accepted 12 July 2021; published 23 July 2021)

The individual difference, particularly in drivers' distance perception, is introduced in the microscopic one-dimensional optimal velocity model to investigate its effect on the onset of the jamming instability seen in traffic systems. We show analytically and numerically that the individual difference helps to inhibit the traffic jam at high vehicle densities while it promotes jamming transition at low vehicle densities. In addition, the jamming mechanism is further investigated by tracking how the spatial disturbance travels through traffics. We find that the jamming instability is uniquely determined by the overall distribution of drivers' distance perception rather than the spatial ordering of vehicles. Finally, a generalized form of the optimal velocity function is considered to show the universality of the effect of the individual difference.

DOI: [10.1103/PhysRevE.104.014311](https://doi.org/10.1103/PhysRevE.104.014311)**I. INTRODUCTION**

One of the most fascinating features of interacting self-driven many-particle systems (i.e., active systems) is that they may exhibit a spontaneous phase transition from a uniform state into an inhomogeneous state [1,2]. The traffic system as one of the well-studied active systems, of which the study dates back to the early 20th century, has perfectly illustrated the dynamical transition to a jammed state even before the road capacity is reached, as everyone experiences on a daily basis [3,4]. The jamming transition could be attributed to various factors such as car accidents, traffic bottlenecks, etc. And, sometimes, the traffic jam could also occur for no apparent reasons, which is known as the “phantom traffic jam.”

To understand the dynamics of traffic systems, mathematical models from different perspectives, such as microscopic particle-based models [5–13], mesoscopic Boltzmann-like models [14,15], and macroscopic continuum models [16–18], have been developed. One of the microscopic models, the so-called optimal velocity model, was proposed by Bando *et al.* [9], where a headway-dependent optimal velocity is introduced in the equation of motion, and the individual difference of drivers is discarded for simplicity. Bando *et al.* showed analytically and numerically that traffic congestion is spontaneously induced as the relaxation time of drivers is slower than the rate of change in the optimal velocity as the distance to the vehicle in the front changes. In addition, Bando *et al.* showed that the inhomogeneous state formed in the model is composed of two different states: a free flow state and a congested state with two specific propagation velocities, which is consistent with the observation of highway traffic [19–21]. Nevertheless, it is worth noting that simplifications such as a closed-loop single-lane traffic are employed in this model. Besides the headway-dependent optimal velocity, there are other realistic factors considered in different traffic models,

such as the relative-velocity dependent optimal velocity [12], the lane-changing effect in a multilane traffic system [22,23], the size effect due to multispecies vehicles [24–27], spatial inhomogeneities in roads [28,29], the temperament of drivers [30,31], etc.

Nonetheless, the assumption of identical drivers is commonly employed in traffic models for simplicity. However, recent researchers show that the complexity of human behaviors could have significant effects on the stability of active systems. For instance, the physical and psychological abilities of drivers may vary over time, which can be described as a stochastic process, and the influence of stochasticity on the stability of traffic systems has been investigated [32–34]. In addition, drivers are expected to perceive the change of surroundings differently, as one would expect for biological beings in general. Previous research shows that heterogeneous traffic flow that is composed of different groups of vehicles also influences the stability of traffic systems [35,36]. Other heterogeneous traffic systems have also been studied [37–41]. Furthermore, it is shown that a wide scattering of synchronized states seen in the fundamental diagram can be reproduced for a traffic model considering a mixture of different vehicle types like cars and trucks, which indicates the importance of the individual difference [26]. Recent study by Tang *et al.* incorporated the individual difference of drivers' perception ability in the macroscopic continuum model to show that scattered data seen in the fundamental diagram could be partly attributed to the individual difference [42].

In this study, we investigate the effect of the individual difference, particularly in drivers' distance perception, on jamming transition using Bando's microscopic model. We show analytically and numerically that the individual difference affects the phase transition significantly, and the individual difference always suppresses traffic jams at high vehicle densities in our discussion. Furthermore, we find, interestingly, by tracking the propagation of the distance disturbance through traffics, that the spatial ordering of drivers is irrelevant to the jamming transition.

<sup>\*</sup>kuoan@phys.nthu.edu.tw

This paper is organized as follows: In Sec. II we briefly review the optimal velocity model by Bando *et al.* In Sec. III the individual difference in drivers' distance perception is introduced using Gaussian random fields, and a linear stability analysis together with a perturbation theory are employed to investigate the effect of the individual difference on the jamming transition quantitatively. To further understand the jamming mechanism, we take a closer look at how a headway disturbance travels through the traffic. We find that the jamming transition is closely related to the overall distribution of drivers' distance perception rather than the spatial ordering of vehicles. Finally, we extend the optimal velocity model to show the universality of the effect of the individual difference in Sec. IV.

## II. OPTIMAL VELOCITY MODEL

In 1995 Bando *et al.* proposed a well-known optimal velocity model involving  $N$  vehicles in a closed loop of length  $L$ , in which the driver of the  $n$ th vehicle adjusts its velocity  $v_n$  according to its distance to the vehicle in front,  $\Delta x_n = x_{n+1} - x_n$ , where  $x_n$  is the location of the  $n$ th vehicle [9]. In this model, a single-lane traffic is considered, and vehicles are not allowed to pass others. The acceleration rule is based on the relaxation dynamics,

$$\ddot{x}_n = \frac{V(w\Delta x_n) - \dot{x}_n}{\tau}, \quad (1)$$

where  $V(w\Delta x_n)$  is the so-called optimal (desired) velocity function, and  $\tau$  is the relaxation time. A simple optimal velocity function introduced by Bando *et al.* is

$$V(w\Delta x_n) = \tanh(w\Delta x_n - h) + \tanh(h). \quad (2)$$

It is clear that the desired velocity of the driver approaches zero as  $\Delta x_n \rightarrow 0$ , so as to avoid car accidents. On the other hand, if there is no vehicle in front, the desired velocity saturates to a certain maximum value. Two parameters,  $w$  and  $h$ , are chosen to describe desired behaviors of drivers. The shift of the hyperbolic tangent function,  $h$ , is used to set the general dependence of the optimal velocity on the interval between vehicles. The parameter  $w$  characterizes the perception of spatial distance of drivers, and it is set to be unity in Ref. [9]. It is evident that drivers with a larger value of  $w$  (poor distance perception) change their desired velocity more abruptly than those with a smaller value of  $w$  (good distance perception) when the distance to the vehicle in front decreases by the same amount, and  $w$  is always positive.

The dynamical behavior of the optimal velocity model is readily obtained by employing the linear stability analysis around the homogeneous steady state. For identical drivers, the homogeneous steady state is

$$x_n^{(0)}(t) = nb + V(wb)t, \quad (3)$$

where  $b = L/N$  is the distance between vehicles, and  $V(wb)$  is the homogeneous steady-state velocity. Now by assuming a small perturbation around the steady state,  $x_n(t) = x_n^{(0)} + y_n(t)$ , and substituting it into Eq. (1), a linearized equation of  $y_n(t)$  is obtained straightforwardly,

$$\ddot{y}_n + \frac{1}{\tau}\dot{y}_n = \frac{f_0}{\tau}w\Delta y_n, \quad (4)$$

where

$$f_0 \equiv \left. \frac{1}{w} \frac{\partial V(w\Delta x_n)}{\partial \Delta x_n} \right|_{\Delta x_n=b}. \quad (5)$$

Due to the periodic boundary condition of a closed loop, the perturbation is expanded in a Fourier series,

$$y_n(t) = \sum_{k=-N/2+1}^{N/2} \tilde{y}_k(t) e^{i\alpha_k n}, \quad (6)$$

where  $\alpha_k = 2\pi k/N$ . Together with Eq. (4), we get  $N$  independent equations,

$$\ddot{\tilde{y}}_k + \frac{1}{\tau}\dot{\tilde{y}}_k = \frac{f_0}{\tau}w\tilde{y}_k[\exp(i\alpha_k) - 1], \quad (7)$$

of which the eigenvalue with the largest real part determines the onset of the instability. Bando *et al.* showed that the homogeneous steady state is unstable when

$$f_0 > \frac{1}{2\tau w \cos^2(\alpha_1/2)}, \quad (8)$$

which is reduced to  $f_0 > (2\tau w)^{-1}$  in the thermodynamic limit.

The physical interpretation of the instability condition is associated with two competing timescales,  $\tau$  and  $1/(2f_0w)$ , respectively, in this model. The first timescale is  $\tau$ , which is the relaxation time. The second timescale is  $1/(2f_0w)$ , which characterizes how fast the desired velocity changes as the distance varies. When the relaxation time  $\tau$  is larger than  $1/(2f_0w)$ , one cannot adjust the velocity fast enough to match one's desired velocity, which is when the jamming instability occurs.

## III. INDIVIDUAL DIFFERENCE

In the original optimal velocity model, one assumes that all drivers obey the same acceleration rules. However, in reality, drivers exhibit different levels of distance perception, hence different degrees of abruptness for drivers to adjust the velocity are to be expected. In this section, we introduce individual difference, specifically the difference in distance perception, to the optimal velocity model. We show that individual difference in distance perception helps to prevent traffic jams in the heavy traffic regime as discussed in detail below.

### A. Linear stability analysis

The individual difference is introduced into the optimal velocity model by assigning a different value of  $w$  to each driver. Therefore, Eq. (1) becomes

$$\ddot{x}_n = \frac{V(w_n\Delta x_n) - \dot{x}_n}{\tau}, \quad (9)$$

where

$$V(w_n\Delta x_n) = \tanh(w_n\Delta x_n - h) + \tanh(h). \quad (10)$$

It is apparent that even if  $\Delta x_n$ 's are the same, drivers would still have different desired velocity  $V(w_n\Delta x_n)$  due to different distance perception. Although drivers are different from one another, it does not seem too far-fetched to assume a simple

Gaussian distribution for  $w_n$ . For simplicity, we assume a Gaussian distribution for  $w_n$  with mean  $\bar{w} = 1$  and standard deviation  $\sigma$ . The steady state of the system is obtained by requiring  $\dot{x}_n = 0$  in Eq. (9). That is, all drivers are moving with the same velocity but with a different distance to the vehicle in front. We obtain

$$x_n^{(0)} = \sum_{i=1}^n \Delta x_i^{(0)} + v^{(0)}t, \quad (11)$$

where we set the location of the first vehicle to be at the origin of the moving frame, and

$$\Delta x_i^{(0)} = \frac{L}{w_i} \left( \sum_j \frac{1}{w_j} \right)^{-1}, \quad (12)$$

$$v^{(0)} = V(w_n \Delta x_n^{(0)}). \quad (13)$$

Similarly, we assume a perturbation  $y_n(t)$  around the steady state, hence the location of the  $n$ th vehicle is  $x_n(t) = x_n^{(0)} + y_n(t)$ . Then the linearized equation of  $y_n(t)$  is readily obtained,

$$\ddot{y}_n + \frac{1}{\tau} \dot{y}_n = \frac{f_1}{\tau} w_n \Delta y_n, \quad (14)$$

where

$$f_1 = \frac{1}{w_n} \frac{\partial V(w_n \Delta x_n)}{\partial \Delta x_n} \Big|_{\Delta x_n = \Delta x_n^{(0)}} = \text{sech}^2(w_n \Delta x_n^{(0)} - h). \quad (15)$$

Substituting the Fourier expansion of  $y_n(t)$ , Eq. (6), into Eq. (14), we obtain

$$\ddot{\tilde{y}}_k + \frac{1}{\tau} \dot{\tilde{y}}_k = \frac{f_1}{\tau} \sum_{\ell} \tilde{y}_{\ell} \tilde{w}_{k-\ell} [\exp(i\alpha_{\ell}) - 1], \quad (16)$$

where  $\tilde{w}_m$  is the  $m$ th Fourier amplitude of the Fourier transform of  $w_n$ 's,

$$w_n = \sum_{m=-N/2+1}^{N/2} \tilde{w}_m e^{i\alpha_m n}. \quad (17)$$

It is interesting to note that Eq. (16) shows an intricate coupling between the dynamics of perturbations and the spatial distribution of different distance perception of drivers. It becomes an eigenvalue problem of coupled equations with  $N$  degrees of freedom. The eigenvalues clearly depend on how  $w_n$ 's are distributed. To generate spatially random and uncorrelated  $w_n$ 's, we employ the Gaussian random field with mean  $\bar{w}$  and standard deviation  $\sigma$ . The Gaussian random field is much easier to be produced in the Fourier space (see Ref. [43]); the ensemble average of the squared magnitude of the Fourier amplitude of the individual difference  $\tilde{w}_k$  ( $k \neq 0$ ) is associated with  $\bar{w}$  and  $\sigma$ ,

$$\langle |\tilde{w}_{k \neq 0}|^2 \rangle = \int \tilde{w}_k \tilde{w}_k^* \prod_i \exp \left[ -\frac{(w_i - \bar{w})^2}{2\sigma^2} \right] dw_i \\ \Big/ \int \prod_i \exp \left[ -\frac{(w_i - \bar{w})^2}{2\sigma^2} \right] dw_i = \frac{\sigma^2}{N}. \quad (18)$$

It shows that the Fourier amplitude of the nonzero wave number mode would be much smaller than that of the zero wave number mode as  $N$  gets larger. Therefore, we can analyze the system perturbatively by separating the coupling terms into an

unperturbed part which is associated only with  $\tilde{w}_0$  (note that  $\tilde{w}_0 = \bar{w}$ ) and a perturbed part which is associated with  $\tilde{w}_{k \neq 0}$ . By defining  $\tilde{\mathbf{y}}^T = (\tilde{y}_{-N/2+1}, \tilde{y}_{-N/2+2}, \dots, \tilde{y}_{N/2})$ , Eq. (16) can be rewritten as

$$\frac{d^2}{dt^2} \tilde{\mathbf{y}} + \frac{1}{\tau} \frac{d}{dt} \tilde{\mathbf{y}} = \frac{f_1}{\tau} (H^0 + H^1) \tilde{\mathbf{y}}, \quad (19)$$

where

$$H_{k\ell}^0 = \tilde{w}_0 [\exp(i\alpha_{\ell}) - 1] \delta_{k\ell},$$

$$H_{k\ell}^1 = \tilde{w}_{k-\ell} [\exp(i\alpha_{\ell}) - 1] (1 - \delta_{k\ell}). \quad (20)$$

Obviously,  $H^0$  is treated as the unperturbed diagonal matrix, while  $H^1$  is treated as the perturbed off-diagonal matrix. The eigenvalues of the unperturbed matrix are exactly the eigenvalues for the original optimal velocity model where the individual difference is absent. Note that, for each realization of the Gaussian random field,  $f_1 = \text{sech}^2(w_n \Delta x_n^{(0)} - h)$  would be slightly different due to the finite size effect. However, if the variance of the Gaussian distribution is small, we can approximate Eq. (12) as

$$w_n \Delta x_n^{(0)} = L \left( \sum_j \frac{1}{w_j} \right)^{-1} \approx \frac{L \tilde{w}_0}{N[1 + (\sigma/\tilde{w}_0)^2]}, \quad (21)$$

which always leads to a smaller value compared to the case of identical drivers ( $\sigma = 0$ ). Therefore, a different value of  $f_1$  is expected, and the neutral stability boundary of the system would differ from that for identical drivers.

Next, we proceed to discuss the correction to eigenvalues due to  $H^1$ . The stability analysis for the original optimal velocity model shows that the most unstable Fourier mode occurs for the longest finite wavelength mode; see Eq. (8). Since the perturbation does not affect the system dramatically, the stability of the system can be determined once the correction to the eigenvalue for the longest finite wavelength mode is known. The first-order correction vanishes, since  $\langle \phi_1 | H^1 | \phi_1 \rangle = 0$  due to the fact that  $H^1$  is an off-diagonal matrix and  $|\phi_1\rangle$  is an eigenvector composed solely of  $\tilde{y}_1$ . The second-order correction to the eigenvalue is  $\lambda_1^{(2)}$ ,

$$\lambda_1^{(2)} = \sum_{k \neq 1} \frac{|\tilde{w}_{1-k}|^2 (e^{i\alpha_k} - 1)(e^{i\alpha_1} - 1)}{\tilde{w}_0 (e^{i\alpha_1} - e^{i\alpha_k})} \simeq -\frac{i\sigma^2}{\tilde{w}_0} \sin \alpha_1. \quad (22)$$

Hence, the governing equation of  $\tilde{y}_1$  [see Eq. (19)] up to second-order perturbation is

$$\ddot{\tilde{y}}_1 + \frac{1}{\tau} \dot{\tilde{y}}_1 \simeq \frac{f_1}{\tau} \tilde{w}_0 \left[ \cos \alpha_1 - 1 + i \left( 1 - \frac{\sigma^2}{\tilde{w}_0^2} \right) \sin \alpha_1 \right], \quad (23)$$

and the instability condition is modified accordingly,

$$f_1 > \frac{1}{2\tau \tilde{w}_0 (1 - \sigma^2/\tilde{w}_0^2)^2 \cos^2(\alpha_1/2)}, \quad (24)$$

which is reduced to  $f_1 > [2\tau \tilde{w}_0 (1 - \sigma^2/\tilde{w}_0^2)^2]^{-1}$  in the thermodynamic limit. Note that  $f_1$  also depends on  $\sigma^2/\tilde{w}_0^2$  since it is a function of  $w_n \Delta x_n^{(0)}$ ; see Eq. (21). Therefore, it is expected that the neutral stability boundary varies as a function of  $\sigma^2/\tilde{w}_0^2$  according to the above perturbation calculation. Figure 1 shows how the phase boundary changes with the individual difference. The threshold value of the relaxation

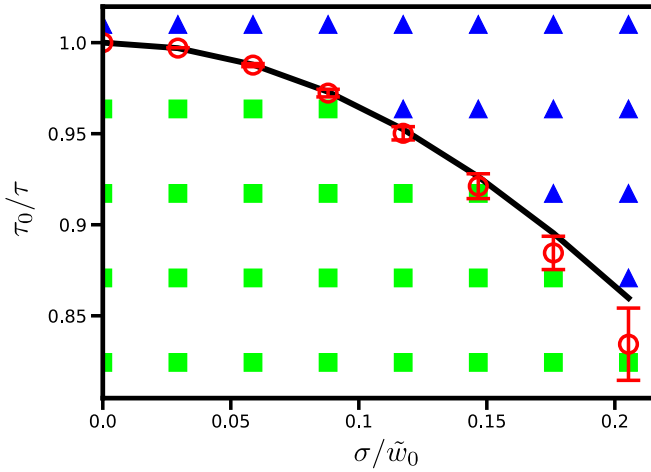


FIG. 1. Phase diagram of the traffic system. Note that  $\tau_0$  is the threshold value of the relaxation time when the individual difference is absent (i.e.,  $\sigma = 0$ ). The black line plots the neutral stability boundary of Eq. (24). Solid green squares and solid blue triangles represent the jammed and unjammed state, respectively, predicted from Eq. (24). Red circles are the simulation results of Eq. (9), which is consistent with the prediction obtained by solving the eigenvalue problem (not shown) of the coupled Eqs. (16). One hundred realizations of Gaussian random fields are carried out for each simulation data point. The phase diagram is obtained for  $N/L = 1$ ,  $h = 2$ , and  $N = 512$ .

time  $\tau$  of drivers increases as  $\sigma/\tilde{w}_0$  increases for a specific vehicle density  $N/L = 1$ . At this vehicle density and for a nonvanishing value of  $\sigma/\tilde{w}_0$ , a higher threshold of relaxation time of drivers is expected, which means the traffic system would remain unjammed even if it takes a longer time for drivers to adjust their velocities. In other words, the variation of distance perception of drivers helps to inhibit the onset of the traffic jam. As shown in Fig. 1, the area of the jammed state on the phase diagram reduces with  $\sigma/\tilde{w}_0$ , and the phase boundary is shown to vary quadratically with  $\sigma/\tilde{w}_0$ . A quantitative analysis is shown in detail in the following section.

Note that the simulation results are obtained using Eq. (9) with a fourth-order Runge-Kutta method. To ensure the simulation accuracy, we employ an adaptive time step which is one hundredth of the minimal value of  $\Delta x_n/v_n$  at each instant. The initial condition of position of vehicles used in simulations is set to be their equilibrium positions along with a small perturbation.

The physical mechanism of the traffic jam can be analyzed by tracking how a spatial disturbance of the location of a vehicle,  $y_n$ , propagates through traffics. Since drivers adjust their speed according to the distance to the vehicle in front, the spatial disturbance of the location of one vehicle would give rise to a wave of disturbances traveling backward. Drivers with poor distance perception (larger  $w$ ) tend to accelerate (or decelerate) more abruptly and overcorrect their speed. Therefore, the amplification of the spatial disturbance is expected if more poor distance perception drivers are in the traffic, which eventually leads to a traffic jam. On the other hand, the drivers with good distance perception (smaller  $w$ ) would reduce the

disturbance and keep the system stable. A quantitative analysis is given as follows.

## B. Propagation of disturbances

Now consider a system composed of  $N$  drivers with different  $w_n$  in a closed loop. All drivers are initially at their equilibrium locations, except the  $n$ th driver whose location is slightly off by the amount of  $y_n$ . Since all vehicles are in a closed loop, the spatial disturbance is expected to travel back to itself repeatedly. Therefore, one can assume  $y_n = A_n(t)e^{i\Omega t} + \text{c.c.}$ , where  $A_n(t)$  is the amplitude of the disturbance wave and  $\Omega$  characterizes the angular frequency of the wave; see Ref. [6].

Since we are looking for the stability of the system near the neutral stability boundary,  $A_n$  is expected to vary on a much slower timescale compared to  $1/\Omega$ . Therefore, by assuming a negligible time derivative of  $A_n$  on the timescale  $1/\Omega$ , we readily obtain, from Eq. (14), the disturbance propagation relation between  $A_{n-1}$  and  $A_n$ ,

$$A_{n-1} = \frac{f_1 w_{n-1}}{R_{n-1}} e^{-i\theta_{n-1}} A_n, \quad (25)$$

where

$$R_{n-1} = \sqrt{(f_1 w_{n-1} - \Omega^2 \tau)^2 + \Omega^2}, \quad (26)$$

$$\theta_{n-1} = \tan^{-1} \left( \frac{\Omega}{f_1 w_{n-1} - \Omega^2 \tau} \right). \quad (27)$$

After the disturbance propagates through the traffic and come back to the  $n$ th vehicle, the amplitude  $A_n$  is amplified by a factor of  $z \equiv \prod_{j=1}^N (f_1 w_j / R_j)$ . Note that we have employed the fact that the sum of the phase difference  $\theta_j$  over all vehicles is simply  $2\pi$ . If  $z$  is greater than unity, the traffic jam occurs. Since the angular frequency of the wave decreases as the number of vehicles increase, in the thermodynamic limit,  $z$  can be well approximated by an expansion in terms of  $\Omega^2$  to the lowest order,

$$\begin{aligned} z &= \prod_n \frac{f_1 w_n}{\sqrt{(f_1 w_n - \Omega^2 \tau)^2 + \Omega^2}} \\ &\simeq 1 - \frac{N}{2(f_1 \tilde{w}_0)^2} \left[ \left( 1 + 3 \frac{\sigma^2}{\tilde{w}_0^2} \right) - 2\tau(f_1 \tilde{w}_0) \left( 1 + \frac{\sigma^2}{\tilde{w}_0^2} \right) \right] \Omega^2. \end{aligned} \quad (28)$$

By requiring  $z > 1$ , it gives the criterion for the instability to occur,

$$f_1 > \frac{1}{2\tau \tilde{w}_0} \left( 1 + 2 \frac{\sigma^2}{\tilde{w}_0^2} \right) + O\left( \frac{\sigma^4}{\tilde{w}_0^4} \right), \quad (29)$$

which is consistent with Eq. (24) to the lowest order of  $(\sigma/\tilde{w}_0)^2$  in the thermodynamic limit. To further explore the individual difference effect on the instability quantitatively, we expand  $f_1$  in terms of  $(\sigma/\tilde{w}_0)^2$ . The neutral stability boundary is readily obtained to the lowest order of  $(\sigma/\tilde{w}_0)^2$ ,

$$\frac{1}{\tau} = 2 \text{sech}^2(\gamma) + \beta \frac{\sigma^2}{\tilde{w}_0^2}, \quad (30)$$

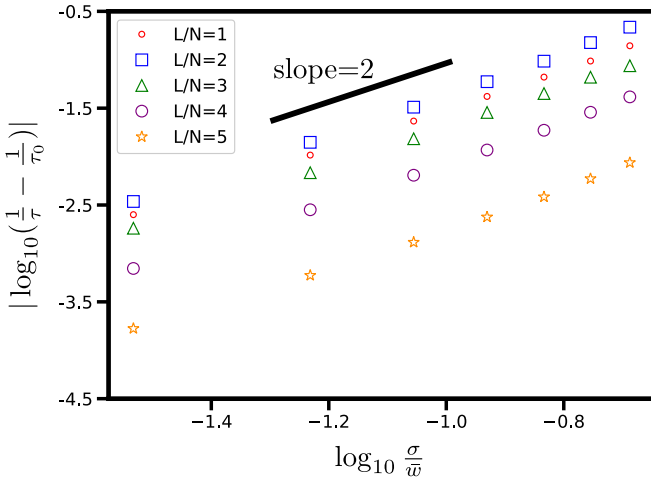


FIG. 2. A log-log plot of simulation results of the deviation of  $1/\tau$  from  $1/\tau_0$  as a function of  $\sigma/\bar{w}_0$  for various global vehicle densities ranging from  $N/L = 0.2$  to  $N/L = 1$ . The simulation results are well fitted by a power-law relation with an exponent of 2. The simulation results are obtained with parameters  $h = 2$  and  $N = 512$ .

where

$$\gamma = \frac{L\tilde{w}_0}{N},$$

$$\beta = 4\text{sech}^2(\gamma - h)[\gamma \tanh(\gamma - h) - 1]. \quad (31)$$

The inverse of the threshold value of the relaxation time  $\tau$  is expected to exhibit a power-law relation with  $(\sigma/\bar{w}_0)$ . Simulation results for 512 vehicles of various densities are shown in Fig. 2; the inverse of the threshold value of  $\tau$  is shown to be well fitted by a quadratic relation of  $\sigma/\bar{w}_0$  for  $\sigma/\bar{w}_0 < 0.2$ . It is interesting to note that the individual difference inhibits the onset of jamming instability at high vehicle densities where  $\beta < 0$ . Below a critical density where  $\beta > 0$ , the individual difference promotes the jamming transition instead.

Figure 3 shows how  $\beta$  changes with the inverse of the vehicle density. The value of  $\beta$  is always negative at high vehicle densities and positive at low vehicle densities regardless of the shift  $h$  of the velocity function, which can be understood as follows. The steady-state velocity of vehicles for drivers with different distance perception is a bit smaller than that for identical drivers; see Eq. (21). Since the onset of the instability comes down to the competition of driver's relaxation time and how fast the desired velocity changes as distance to the front varies, at high vehicle densities, the rate change of the desired velocity is less sensitive to the distance change which inhibits the traffic jam. On the other hand, at low vehicle densities, drivers tend to brake or accelerate more abruptly as the distance to the front changes, which makes the traffic system more vulnerable to the traffic jam.

### C. Irrelevance of spatial ordering of vehicles

In the above analysis of disturbance propagation, the stability of a traffic system depends on the amplifying factor  $z$  [see Eq. (28)], which involves a product of  $w_j/R_j$  of each vehicle. Since the product is invariant as one switches the spatial ordering of vehicles, the jamming transition of traffic systems is

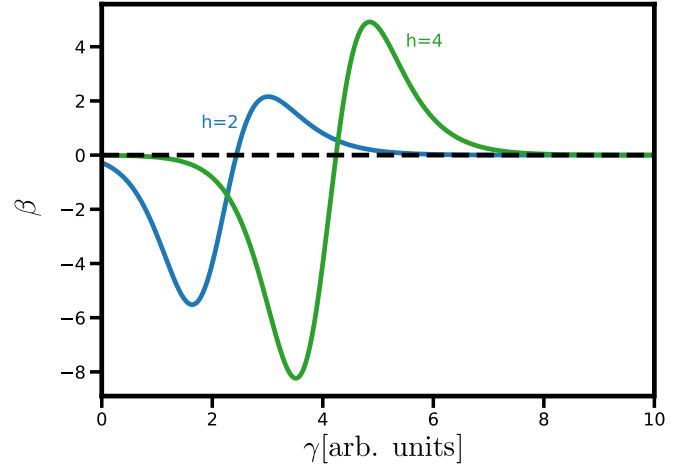


FIG. 3. Plot of the coefficient  $\beta$  as a function of  $\gamma$  for different values of  $h$ .  $\beta$  is always negative at high vehicle densities, which inhibits the jamming transition, while  $\beta$  becomes positive at low vehicle densities, which promotes the jamming transition. The value of  $h$  characterizes the rate change of the velocity function as the headway changes, which uniquely determines the critical vehicle density at which  $\beta = 0$ .

uniquely determined for the same group of drivers regardless of their spatial ordering. One could reach the same conclusion by solving the eigenvalue problem formulated before; see Eq. (14). For a given set of  $w_n$ 's, the characteristic equation remains invariant as one reshuffles the spatial ordering of vehicles.

Figure 4 shows the simulation results of the amplitude for the slowest decaying eigenvector over time for 16 vehicles. The numerical simulations are carried out in the unjammed region that is close to the neutral stability boundary, and six different configurations of the spatial ordering of vehicles

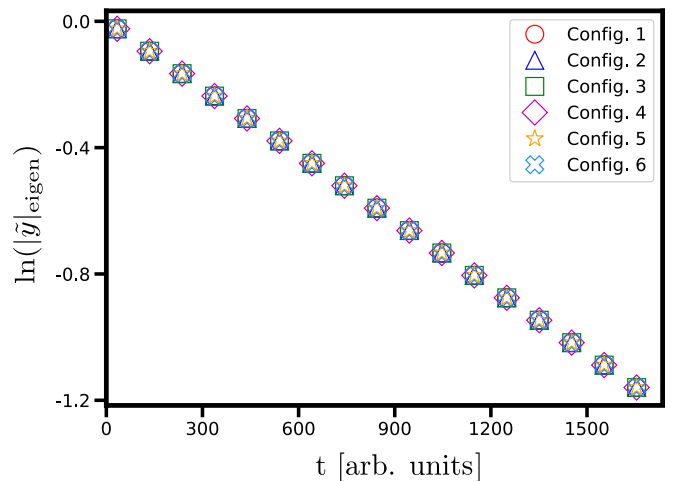


FIG. 4. The amplitude of the slowest decaying eigenvector over time for simulations of 16 vehicles,  $N/L = 1$ ,  $\sigma/\bar{w}_0 = 0.176$ , and  $\tau = 1.096$  in the unjammed region. Six different spatial configurations are generated by reshuffling the ordering of vehicles. Different symbols represent different configurations. Note that the amplitude oscillates with time, and only the peak values are shown.

generated by random reshuffling are employed. In the linear regime, simulations show that dynamical behaviors for the slowest decaying eigenvector are identical for all six configurations. It is interesting to note that our calculation indicates that the stability of the traffic systems would be the same even for traffic systems that allow vehicles to switch order.

#### IV. UNIVERSALITY OF THE EFFECT OF INDIVIDUAL DIFFERENCE

It is intuitive that, in addition to the relative distance, the relative velocity to the vehicle in the front would also influence drivers' action to accelerate or decelerate. Based on the concept shown in Refs. [12,44], we propose a generalized traffic model incorporated with the individual difference,

$$\ddot{x}_n = \frac{1}{\tau} [V_1(w_n \Delta x_n) + \lambda V_2(g_n \Delta v_n) e^{-w_n \Delta x_n / R} - \dot{x}_n], \quad (32)$$

where  $V_1$  is the same optimal velocity function introduced before,  $V_1(w_n \Delta x_n) = \tanh(w_n \Delta x_n - h) + \tanh(h)$ . And the second term is the additional acceleration due to the relative velocity, where

$$V_2(g_n \Delta v_n) = \tanh(g_n \Delta v_n), \quad (33)$$

so that the driver slows down (speeds up) when its velocity is faster (slower) than the vehicle in the front. Note that  $w_n$ 's and  $g_n$ 's are populated with Gaussian random fields with mean  $\bar{w}$  and  $\bar{g}$ , and standard deviation  $\sigma_w$  and  $\sigma_g$ , respectively. The exponential decay term describes the distance-dependent interaction to the vehicle in the front, and  $R$  characterized the interaction length. It is clear that, at higher vehicle densities, the acceleration due to the relative velocity is more pronounced since  $w_n \Delta x_n / R$  is relatively smaller. Finally,  $\lambda$  represents the relative strength of the influence of the second term to the first term.

We employ the same disturbance propagation analysis to calculate the neutral stability boundary of this system. In the thermodynamic limit, and to the lowest order expansion of  $(\sigma_w / \bar{w}_0)^2$  and  $(\sigma_g / \bar{g}_0)^2$ , the onset of the instability occurs when

$$f_1 > \frac{1}{2\tau \bar{w}_0} \left( 1 + \frac{2\sigma_w^2}{\bar{w}_0^2} \right) + \frac{\lambda \bar{g}_0}{\tau \bar{w}_0} \left[ 1 + \frac{2\sigma_w^2}{\bar{w}_0^2} - \frac{2\text{Cov}(w, g)}{\bar{w}_0 \bar{g}_0} \right] \times e^{-w_n \Delta x_n^{(0)} / R}, \quad (34)$$

where  $\text{Cov}(w, g)$  is the covariance of  $w_n$  and  $g_n$ . In the limit  $\lambda \rightarrow 0$ , Eq. (34) simply rediscovers the instability criterion derived in Eq. (29). First, let us consider the case where  $w_n$  and  $g_n$  are independent from each other, which means individual's distance perception is uncorrelated to individual's relative velocity perception, hence,  $\text{Cov}(w, g) = 0$ . The neutral stability boundary as a function of  $(\sigma_w / \bar{w}_0)^2$  is shown in Fig. 5. At high vehicle densities, the individual difference further inhibits the jamming transition as the relative velocity dependent acceleration rule is considered. The unjammed phase space opens up while the jammed phase space is further suppressed as the variation of distance perception increases; see the comparison of Fig. 1 and Fig. 5. It is quite intuitive since, if the distance to the vehicle in the front is close, the relative velocity dependent acceleration would slow down the

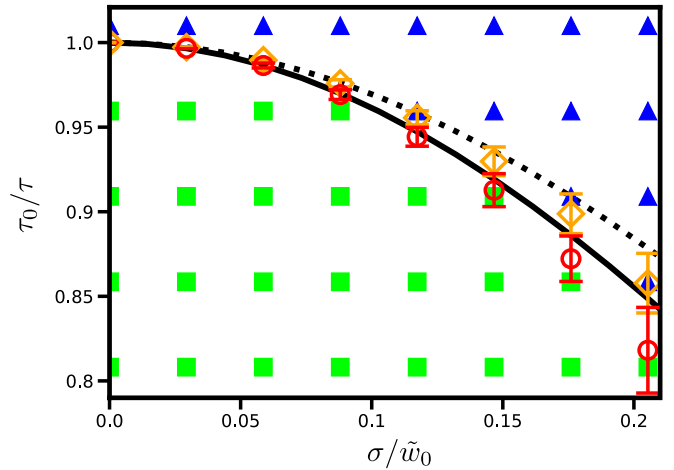


FIG. 5. Phase diagram of the traffic system shown in Eq. (32). The black line plots the neutral stability boundary of Eq. (34) for  $\text{Cov}(w, g) = 0$ , and solid green squares and solid blue triangles represent the jammed and unjammed states, respectively. Numerical simulations of Eq. (32) for  $\text{Cov}(w, g) = 0$  are shown in red circles. Orange diamonds and dotted line represent the result of simulations and analytical results, respectively, for the scenario where  $w_n = g_n$ . One hundred realizations of Gaussian random fields are carried out for each simulation data point. The phase diagram is obtained for  $R = 1$ ,  $\lambda = 1$ ,  $N/L = 1$ ,  $h = 2$ , and  $N = 256$ .

vehicle as the vehicle in the front is slower. This mechanism helps to maintain distance between vehicles effectively; therefore, it suppresses the jamming transition. In addition, let us consider the other case where  $w_n$  equals to  $g_n$ , which means the driver who accelerates abruptly due to the change of the relative distance would also accelerate abruptly due to the change of relative velocity, hence,  $\text{Cov}(w, g) = \sigma_g^2 = \sigma_w^2$ . A similar trend of the neutral stability boundary is observed; see Fig. 5. However, the correlation between  $w_n$  and  $g_n$  shrinks the unjammed phase space a little bit, since more abrupt change in the desired velocity makes the system easier to be jammed. On the contrary, it is expected that an anticorrelated  $w_n$  and  $g_n$  would help to inhibit traffic jam.

#### V. SUMMARY AND DISCUSSION

We investigate how the individual difference of drivers affects the jamming instability by implementing different distance perception using Gaussian random fields in Bando's optimal velocity model. Both simulation results and perturbation calculations show that, at high vehicle densities, the onset of the jamming instability is effectively suppressed if the individual difference is introduced. On the other hand, the instability is promoted at low vehicle densities. To further understand the physical mechanism of jamming instability, we analyze how the spatial disturbance in the relative distance propagates through the traffic. We find that drivers with good distance perception reduce the disturbance, while drivers with poor distance perception amplify it. Therefore, we show that whether the instability occurs depends on the overall distribution of the distance perception rather than the detail of the spatial ordering of vehicles. It indicates that the individual

difference of drivers would also suppress the traffic jam for traffic systems that allow vehicles to pass each other.

The universality of individual difference-induced jamming suppression can be further elucidated by considering a more general form of the desired velocity. We get

$$\ddot{x}_n = \frac{V(w_n \Delta x_n, g_n \Delta v_n) - \dot{x}_n}{\tau}, \quad (35)$$

where  $V(w_n \Delta x_n, g_n \Delta v_n)$  is the generalized desired velocity which monotonically increases as the distance to the vehicle in the front increases or as the relative velocity increases. The parameter  $g_n$  is employed to characterize the relative velocity perception of the  $n$ th driver. Employing the disturbance propagation analysis, the onset of the instability occurs when

$$V_x > \frac{1}{\tilde{w}_0 \tau} \left[ \left( 1 + \frac{2\sigma^2}{\tilde{w}_0^2} \right) \left( \frac{1}{2} + V_v \tilde{g}_0 \right) - \frac{2V_v \text{Cov}(w, g)}{\tilde{w}_0} \right], \quad (36)$$

where  $V_x = (\partial V / \partial \Delta x_n) / w_n$  and  $V_v = (\partial V / \partial \Delta v_n) / g_n$ , both evaluated at  $\Delta x_n = \Delta x_n^{(0)}$  and  $\Delta v_n = 0$ . It is clear that the jamming instability is influenced by the individual difference in several different aspects. First, the slight decrease in the steady-state velocity due to the variation of individual distance perception gives rise to a relatively slow change in the desired velocity as the distance changes at high vehicle densities and vice versa, which inhibits and promotes the jamming transition at high and low vehicle densities, respectively. This conclusion is universal since the desired velocity function has to saturate to certain values at both ends of the vehicle density, which warrants an inflection point (density) for the desired velocity function. Therefore, the rate of the change in the desired velocity due to variation of distance perception

would be either smaller or larger depending on the vehicle density. Past work has shown that the inflection point is crucial in analyzing nonlinear wave in the jammed state [13,45–48]. Second, the term  $V_v \tilde{g}_0$  always inhibits the jamming transition, since the relative velocity dependent acceleration would effectively help to maintain proper distance between vehicles. Furthermore, the correlation between the distance perception and relative velocity perception of drivers is shown to affect the jamming transition as well, since the correlation could further enhance the abruptness of the velocity change.

In this study, we show that the individual difference has a pronounced effect on the onset of the jamming instability in the optimal velocity model. It is of interest to extend the current discussion to explore how the individual difference affects the traffic flow in a more realistic system that includes lane changing, traffic bottlenecks, etc. [49]. For a more realistic system, one can investigate whether the individual difference has an effect on the relation between the traffic flow and the vehicle density (i.e., the fundamental diagram). Since we have shown that the variation of distance perception leads to changes in the steady-state velocity, therefore, the individual difference could be responsible for the wide scattering nature of the fundamental diagram.

#### ACKNOWLEDGMENTS

The authors thank M.-W. Liu for helpful discussions. We gratefully acknowledge the support of the Ministry of Science and Technology, Taiwan (Grant No. MOST 109-2112-M-007-005-) and the support from the National Center for Theoretical Sciences, Taiwan.

- 
- [1] M. E. Cates and J. Tailleur, Motility-induced phase separation, *Annu. Rev. Condens. Matter. Phys.* **6**, 219 (2015).
  - [2] M. C. Marchetti, J. F. Joanny, S. Ramaswamy, T. B. Liverpool, J. Prost, M. Rao, and R. A. Simha, Hydrodynamics of soft active matter, *Rev. Mod. Phys.* **85**, 1143 (2013).
  - [3] B. Greenshields, J. Bibbins, W. Channing, and H. Miller, A study of traffic capacity, *Highw. Res. Board Proc.* **14**, 448 (1935).
  - [4] D. Helbing, Traffic and related self-driven many-particle systems, *Rev. Mod. Phys.* **73**, 1067 (2001).
  - [5] L. A. Pipes, An operational analysis of traffic dynamics, *J. Appl. Phys.* **24**, 274 (1953).
  - [6] R. E. Chandler, R. Herman, and E. W. Montroll, Traffic dynamics: Studies in car following, *Opns. Res.* **6**, 165 (1958).
  - [7] D. C. Gazis, R. Herman, and R. W. Rothery, Nonlinear follow-the-leader models of traffic flow, *Opns. Res.* **9**, 545 (1961).
  - [8] G. F. Newell, Nonlinear effects in the dynamics of car following, *Opns. Res.* **9**, 209 (1961).
  - [9] M. Bando, K. Hasebe, A. Nakayama, A. Shibata, and Y. Sugiyama, Dynamical model of traffic congestion and numerical simulation, *Phys. Rev. E* **51**, 1035 (1995).
  - [10] K. Nagel and M. Schreckenberg, A cellular automaton model for freeway traffic, *J. Phys. I France* **2**, 2221 (1992).
  - [11] K. Nagel and H. J. Herrmann, Deterministic models for traffic jams, *Physica A* **199**, 254 (1993).
  - [12] D. Helbing and B. Tilch, Generalized force model of traffic dynamics, *Phys. Rev. E* **58**, 133 (1998).
  - [13] T. Nagatani, The physics of traffic jams, *Rep. Prog. Phys.* **65**, 1331 (2002).
  - [14] I. Prigogine and F. C. Andrews, A Boltzmann-like approach for traffic flow, *Opns. Res.* **8**, 789 (1960).
  - [15] S. Paveri-Fontana, On boltzmann-like treatments for traffic flow: A critical review of the basic model and an alternative proposal for dilute traffic analysis, *Transp. Res.* **9**, 225 (1975).
  - [16] M. J. Lighthill and G. B. Whitham, On kinematic waves ii. a theory of traffic flow on long crowded roads, *Proc. R. Soc. Lond. A* **229**, 317 (1955).
  - [17] P. I. Richards, Shock waves on the highway, *Opns. Res.* **4**, 42 (1956).
  - [18] G. B. Whitham, *Linear and Nonlinear Waves* (John Wiley, New York, 1974).
  - [19] M. Bando, K. Hasebe, A. Nakayama, A. Shibata, and Y. Sugiyama, Structure stability of congestion in traffic dynamics, *Jpn. J. Ind. Appl. Math.* **11**, 203 (1994).
  - [20] Y.-b. Sugiyama and H. Yamada, Simple and exactly solvable model for queue dynamics, *Phys. Rev. E* **55**, 7749 (1997).
  - [21] B. S. Kerner and H. Rehborn, Experimental Properties of Phase Transitions in Traffic Flow, *Phys. Rev. Lett.* **79**, 4030 (1997).
  - [22] M. Rickert, K. Nagel, M. Schreckenberg, and A. Latour, Two lane traffic simulations using cellular automata, *Physica A* **231**, 534 (1996).

- [23] P. Wagner, K. Nagel, and D. E. Wolf, Realistic multi-lane traffic rules for cellular automata, *Physica A* **234**, 687 (1997).
- [24] A. D. Mason and A. W. Woods, Car-following model of multi-species systems of road traffic, *Phys. Rev. E* **55**, 2203 (1997).
- [25] B. Tilch and D. Helbing, Evaluation of single vehicle data in dependence of the vehicle-type, lane, and site, in *Traffic and Granular Flow '99*, edited by D. Helbing, H. J. Herrmann, M. Schreckenberg, and D. E. Wolf (Springer, Berlin, 2000), pp. 333–338.
- [26] M. Treiber and D. Helbing, Macroscopic simulation of widely scattered synchronized traffic states, *J. Phys. A* **32**, L17 (1999).
- [27] B. S. Kerner and S. L. Klenov, Spatial-temporal patterns in heterogeneous traffic flow with a variety of driver behavioural characteristics and vehicle parameters, *J. Phys. A* **37**, 8753 (2004).
- [28] D. Helbing, A. Hennecke, and M. Treiber, Phase Diagram of Traffic States in the Presence of Inhomogeneities, *Phys. Rev. Lett.* **82**, 4360 (1999).
- [29] M. Treiber, A. Hennecke, and D. Helbing, Congested traffic states in empirical observations and microscopic simulations, *Phys. Rev. E* **62**, 1805 (2000).
- [30] G. Zhang, D.-H. Sun, H. Liu, and M. Zhao, Analysis of drivers' characteristics in car-following theory, *Mod. Phys. Lett. B* **28**, 1450191 (2014).
- [31] D. Herrero-Fernández, Psychophysiological, subjective and behavioral differences between high and low anger drivers in a simulation task, *Transp. Res. Part F: Traffic Psychol. Behav.* **42**, 365 (2016).
- [32] D. Ngoduy, S. Lee, M. Treiber, M. Keyvan-Ekbatani, and H. Vu, Langevin method for a continuous stochastic car-following model and its stability conditions, *Transp. Res. Part C: Emerg. Technol.* **105**, 599 (2019).
- [33] A. Tordeux and A. Schadschneider, White and relaxed noises in optimal velocity models for pedestrian flow with stop-and-go waves, *J. Phys. A* **49**, 185101 (2016).
- [34] S. H. Hamdar, H. S. Mahmassani, and M. Treiber, From behavioral psychology to acceleration modeling: Calibration, validation, and exploration of drivers' cognitive and safety parameters in a risk-taking environment, *Transp. Res. Part B: Methodol.* **78**, 32 (2015).
- [35] D. Ngoduy, Effect of the car-following combinations on the instability of heterogeneous traffic flow, *Transportmetrica B: Transp. Dyn.* **3**, 44 (2015).
- [36] D.-F. Xie, X.-M. Zhao, and Z. He, Heterogeneous traffic mixing regular and connected vehicles: Modeling and stabilization, *IEEE trans. Intell. Transp. Syst.* **20**, 2060 (2019).
- [37] F. Sun, J. Wang, R. Cheng, and H. Ge, An extended heterogeneous car-following model accounting for anticipation driving behavior and mixed maximum speeds, *Phys. Lett. A* **382**, 489 (2018).
- [38] T. Li, F. Hui, X. Zhao, and D. Ngoduy, Effects of dsrc-based safety messages on heterogeneous traffic flow stability, in *CI-CTP 2019: Transportation in China—Connecting the World* (ASCE, Reston, VA, 2019), pp. 2199–2210.
- [39] S. Ossen and S. P. Hoogendoorn, Heterogeneity in car-following behavior: Theory and empirics, *Transp. Res. Part C: Emerg. Technol.* **19**, 182 (2011).
- [40] A. Tordeux, S. Lassarre, and M. Roussignol, An adaptive time gap car-following model, *Transp. Res. Part B: Methodol.* **44**, 1115 (2010).
- [41] Y. Rong and H. Wen, An extended car-following model considering the appearing probability of truck and driver's characteristics, *Phys. Lett. A* **382**, 1341 (2018).
- [42] T. Tang, C. Li, H. Huang, and H. Shang, A new fundamental diagram theory with the individual difference of the driver's perception ability, *Nonlinear Dyn.* **67**, 2255 (2012).
- [43] T. Hida and M. Hitsuda, *Gaussian Processes* (American Mathematical Society, Providence, RI, 1993).
- [44] J.-F. Tian, B. Jia, and X.-G. Li, A new car following model: Comprehensive optimal velocity model, *Commun. Theor. Phys.* **55**, 1119 (2011).
- [45] T. S. Komatsu and S.-i. Sasa, Kink soliton characterizing traffic congestion, *Phys. Rev. E* **52**, 5574 (1995).
- [46] T. Nagatani, Thermodynamic theory for the jamming transition in traffic flow, *Phys. Rev. E* **58**, 4271 (1998).
- [47] M. Muramatsu and T. Nagatani, Soliton and kink jams in traffic flow with open boundaries, *Phys. Rev. E* **60**, 180 (1999).
- [48] T. Nagatani, Density waves in traffic flow, *Phys. Rev. E* **61**, 3564 (2000).
- [49] B. S. Kerner, *The Physics of Traffic* (Springer-Verlag, Berlin, 2004).